ELSEVIER

Chemical Engineering Journal 86 (2002) 269–276

Chemical Engineering Journal

www.elsevier.com/locate/cej

Analysis of flow patterns in bubble and slurry bubble columns based on local heat transfer measurements

H. Li, A. Prakash*

Department of Chemical and Biochemical Engineering, The University of Western Ontario, London, Ont., Canada N6A 5B9

Received 7 July 2000; received in revised form 16 May 2001; accepted 23 May 2001

Abstract

Flow patterns in two-phase (G–L) and three-phase (G–L–S) bubble columns are investigated based on local time-averaged heat transfer coefficients. The experiments are conducted in a 0.28 m diameter Plexiglas column in air–water and air–water–glass beads (35 μm) systems over superficial gas velocity range 0.05–0.3 m/s and slurry concentration range 0–40 vol.%. The heat transfer measurements are made with a specially designed probe which provided local heat transfer coefficients. The measured heat transfer data are analyzed to illustrate the effects of gas velocities and slurry concentrations on flow patterns in different regions of the column. The heat transfer measurements at different axial and radial positions and for different probe orientations provided further insights into liquid circulation patterns in the column. © 2002 Elsevier Science B.V. All rights reserved.

Keywords: Bubble column; Slurry bubble column; Heat transfer coefficients; Flow patterns; Flow structures

1. Introduction

Several benefits provided by bubble column reactors have made them attractive for a number of industrial applications such as heavy oil upgrading, Fischer–Tropsch synthesis, environmental pollution control and biotechnology [1]. The advantages offered by these reactors include high heat and mass transfer rates, isothermal conditions and on-line catalyst addition and withdrawal. Also, there are low maintenance requirements due to simple construction and absence of any moving parts. A detailed understanding of flow structure and mixing behavior, however, is still lacking for optimal design and scale-up of these reactors. A growing number of literature studies have started addressing these issues to facilitate the design process. For example, attempts have been made to study flow structure in bubble columns using techniques such as particle image velocimetry [2,3], laser Doppler anemometry [4] and single-particle tracking techniques [5–7]. These techniques are generally expensive and require elaborate experimental set up. Moreover, the applicability of literature techniques is mostly limited to gas–liquid systems or dilute suspensions of particles in liquid. This study attempts to describe flow structure in bubble columns based on measurements of local heat transfer coefficients. The heat transfer coefficients were obtained with the help of a fast response probe of sturdy construction. The movable heat transfer probe could provide heat transfer coefficients in different axial, radial and angular positions which provided insights into flow patterns in the column. The probe identified flow direction by comparing stagnation point heat transfer coefficients for different probe orientations. The local liquid or slurry velocities are estimated from stagnation point Nusselt number. The probe also worked well in high slurry concentrations used in this study.

2. Experimental

Experiments were conducted in a Plexiglas column of 0.28 m inside diameter and 2.4 m height (Fig. 1). It consisted of three sections, the bottom and top sections were 0.60 m high and the middle section was 1.2 m tall. A six-arm gas distributor introduced air into the column bottom. Gas distributor arms were 5 mm in diameter and 0.14 m long. Each arm had four 1.5 mm diameter holes facing downwards. An electric heater was installed near the column bottom to maintain a constant bulk temperature.

Tap water was the liquid phase, while compressed air and 35 μm glass beads constituted the gas and solid phases, respectively. Gas flow was measured by a rotameter (Omega

* Corresponding author. Tel.: +1-519-661-2111, ext: 88528; fax: +1-519-661-3498.
E-mail address: aprakas2@julian.uwo.ca (A. Prakash).

1385-8947/02/$ – see front matter © 2002 Elsevier Science B.V. All rights reserved.
PII: S1385-8947(01)00186-3

Nomenclature

a_s	empirical constant in Eq. (3)
C_p	specific heat (J/kg K)
d_p	diameter of cylindrical probe (m)
D_c	column diameter (m)
h	heat transfer coefficient (kW/m^2 K)
h_{avg}	average heat transfer coefficient (kW/m^2 K)
h_i	instantaneous heat transfer coefficient (kW/m^2 K)
h_s	stagnation point heat transfer coefficient (kW/m^2 K)
h_0	heat transfer coefficient at column center (kW/m^2 K)
k	thermal conductivity (kW/m K)
N	number of data points used to obtain time-averaged heat transfer coefficient
p	pressure (Pa)
Pr	Prandtl number for suspension, $C_p\mu/k$
Q	heat flux (kW/m^2)
r	radial distance (m)
R	column radius (m)
ΔT_{si}	temperature difference between sensor surface and bed (K)
$U_{b,\infty}$	terminal bubble rise velocity (m/s)
U_L	local liquid velocity (m/s)
$U_{L,0}$	liquid velocity at column center (m/s)
V_G	superficial gas velocity (m/s)
V_S	hindered particle settling velocity (m/s)
z	axial distance (m)

Greek letters

ε	phase holdup
μ	viscosity (Pa s)
ν	kinematic viscosity (m^2/s)
ρ	density (kg/m^3)

Subscripts

G	gas
L	liquid
S	solids

FL-1660) and superficial gas velocity was varied from 0.05 to 0.30 m/s. The unaerated liquid height was 1.4 m and the temperature was maintained at 23 °C in the column. Copper–constantan thermocouples (Omega TMTSS-032) were arranged at various vertical positions to monitor bed temperature. The instantaneous heat transfer flux was measured by means of a heat flow sensor (RDF, micro-foil heat flow sensor No. 20453-1) flush mounted on the surface of a brass cylinder of 11 mm OD. A small cartridge heater was installed inside the brass cylinder. The details of the probe design are given elsewhere [8,9]. The difference in temperature across the thermal barrier was proportional to heat

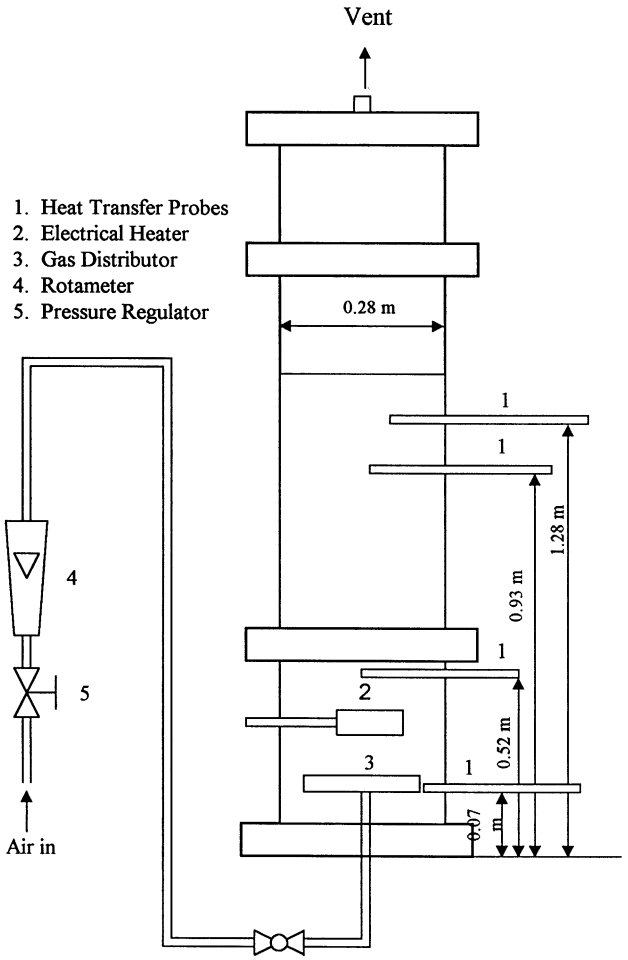

Fig. 1. Schematic diagram of the experimental set up.

flux through the sensor. The sensor output voltage provided the local heat flux and it also measured the probe surface temperature. The construction of the sensor provided fast response time (0.02 s). The heat transfer probes were located at 0.07, 0.52, 0.93 and 1.28 m from the column bottom (Fig. 1). The probes could be moved in and out radially as well as rotated to change the orientation of the heat flux sensor. However, at the axial location of 0.07 m, the probe could not be moved to column center due to interference with air inlet pipe. The signals from the heat flux sensor and surface temperature were collected simultaneously at 60 Hz for about 35 s. The microvolt signals from the heat flux sensor were amplified to millivolt level before collection by data acquisition system. The local instantaneous heat transfer coefficient (h_i) was obtained from the temperature difference between probe surface and the bulk region ΔT_{si} and heat transfer flux Q:

$$h_i = \frac{Q}{\Delta T_{si}} \quad (1)$$

The time-average heat transfer coefficient at a given location was obtained by averaging the instantaneous heat transfer

coefficient data collected

$$h_{\text{avg}} = \frac{1}{N}\sum_{i=1}^{N}\frac{Q}{\Delta T_{\text{si}}} \quad (2)$$

The value of N was selected to be 2100 to establish a stable value of heat transfer coefficient for all conditions.

3. Results and discussion

Fig. 2 presents the heat transfer coefficients obtained in the wall region ($r/R = 0.96$) and central region ($r/R = 0.0$) of the column at different axial locations: 0.07, 0.52, 0.93 and 1.28 m from column bottom. In the wall region, the heat transfer coefficients at the lowest position ($z = 0.07$ m) are lower than higher locations. The local heat transfer coefficients at axial locations of 0.93 and 1.28 m are quite close. For the intermediate location of 0.52 m, the heat transfer coefficients come closer to values at higher elevations with increasing gas velocity. This indicates that with increasing gas velocity flow patterns from higher elevations extend to lower levels in the wall region, but do not seem to reach below the gas distributor. The top two probes were located in the fully developed bulk flow region of the column since no axial variations in local heat transfer coefficients are observed at these locations. The bottom most location provided heat transfer coefficients in the distributor region of the column. It can be seen that heat transfer coefficients in the bulk region are significantly higher than the distributor region and the differences increase with increasing gas velocity. These results point to different mixing patterns in the two regions.

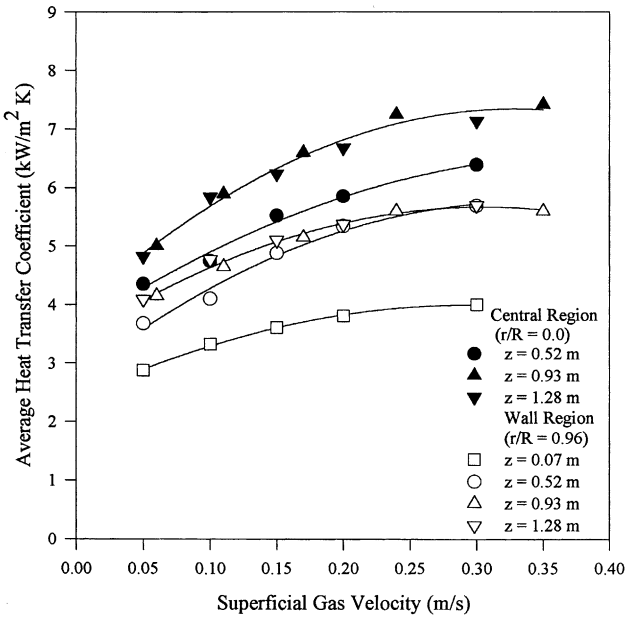

Fig. 2. Comparison of heat transfer coefficients in central and wall regions at different axial positions (slurry concentration, 10 vol.%).

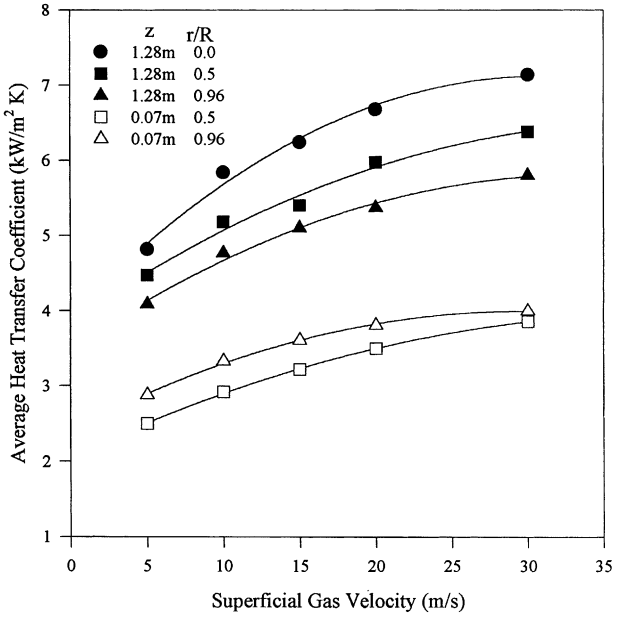

Fig. 3. Variation of heat transfer coefficients with gas velocity in the distributor and the bulk region (slurry concentration, 10 vol.%).

The intermediate location of 0.52 m seems to lie in the region of developing flow structure in between the distributor and the bulk regions. These differences were further explored by comparing heat transfer coefficients in the central region of the column. As shown in Fig. 2, the heat transfer coefficients at the axial location of 0.52 m remained lower than those at higher elevations even at high gas velocities, as opposed to the wall region. These differences indicate that in the developing region, flow structure at the center of the column evolve differently than the wall region. This could be attributed to bubble–bubble interactions and evolving bubble wake region. The growing wake region would pull in the liquid flowing down the wall region, thus reducing its flow into the distributor region.

Fig. 3 compares the effects of gas velocity on heat transfer coefficients at different radial positions in the bulk and the distributor regions. It can be observed that the heat transfer coefficients in the distributor region at the two radial locations come closer with increasing gas velocity. However, in the bulk region the differences between heat transfer coefficients at different radial positions increase with increasing gas velocity. These observations clearly suggest different mixing patterns in the two regions. Mixing in the distributor region could be assumed to be more uniform due to smaller differences in heat transfer coefficients at different radial positions. Visual observations indicated that in the distributor region, mixing was caused mainly by the processes of bubbles and gas jets formations. With increasing gas velocity, gas jets were observed penetrating downwards (from the downward facing orifices) and then turning up with chain of bubbles rising above the distributor. The orifices were arranged on the sparger arm to ensure nearly uniform injection of gas per unit cross-sectional area of the column. This

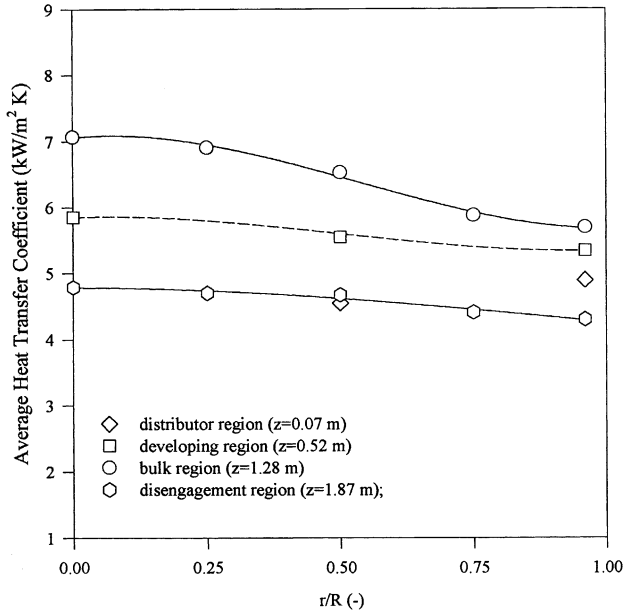

Fig. 4. Comparison of radial heat transfer coefficients at different axial locations (air–water system; $V_G = 0.2\,m/s$).

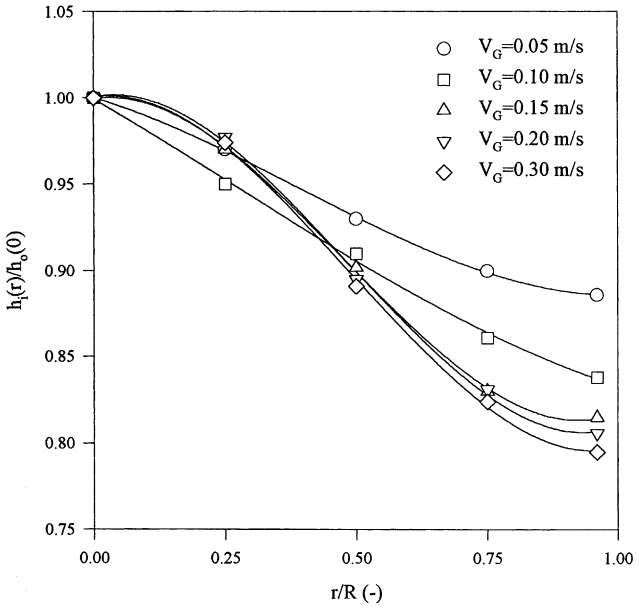

Fig. 5. Radial profiles of normalized heat transfer coefficients in the bulk region for different gas velocities (air–water system).

resulted in closely spaced orifices near the column wall. With increasing gas velocities, the gas jets from adjacent orifices seemed to merge thus creating stronger circulation and mixing in the region. Based on these observations, mixing around the distributor can be attributed to transfer of momentum from gas jets to surrounding area and any entrainment by bubble chain rising above the distributor. Low heat transfer coefficients in the region indicate low level of turbulence in the region. The radial differences in the bulk region could be attributed to bubble wake enhanced heat transfer and large circulation patterns generated by bubble wake effects. A comparison of radial profiles of heat transfer coefficients in different regions of the column shows relatively flat profiles in the developing and disengagement regions compared to the bulk region (Fig. 4). Similarity of radial profiles in the disengagement, the distributor and the developing regions indicate that the overall mixing behavior in these regions could be similar. The actual mixing parameters, however, are expected to be different as indicated by differences in local heat transfer coefficients. Heat transfer coefficients in the disengagement and the distributor regions are close indicating similarity of mixing parameters. The distributor design and its configuration are expected to influence the size of the distributor region to a larger extent and developing region to a lesser extent.

Radial profiles of heat transfer coefficients in the bulk region were further investigated on the effects of gas velocities and slurry concentrations. Fig. 5 compares radial profiles of normalized heat transfer coefficients in air–water system for increasing gas velocities. It can be seen that the radial profiles are similar above gas velocity of 0.1 m/s but are different for lower gas velocities. This indicates similarity of flow patterns in fully developed heterogeneous regime developing above gas velocity of 0.1 m/s in air–water system. In the 20 vol.% slurry system, however, the radial profiles are essentially similar for all gas velocities (Fig. 6). This indicates that onset of the heterogeneous regime begins at a lower velocity in the presence of solid articles. These observations can be compared with the study of Krishna et al. [10] where similar conclusions were reached based on gas holdup measurements. This shows that radial heat transfer

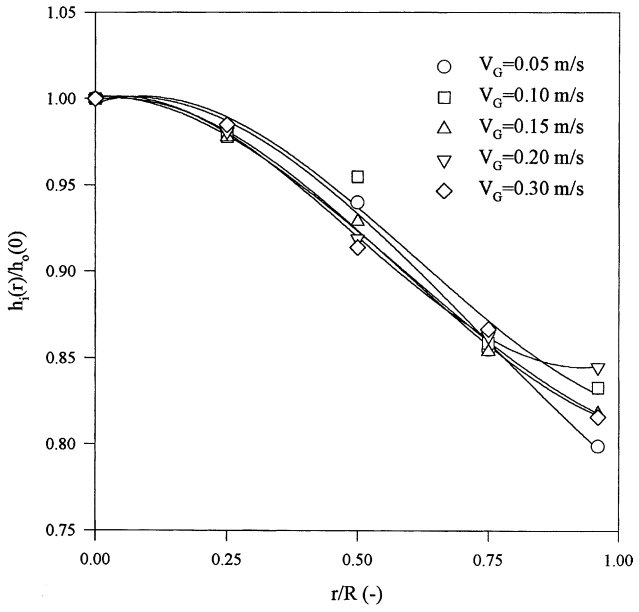

Fig. 6. Radial profiles of normalized heat transfer coefficients in the bulk region for different gas velocities (slurry concentration, 10 vol.%).

profiles could be used to identify transition from one flow regime to another.

The above observations of radial heat transfer coefficients of this study can be related to reported radial profiles of liquid velocity and gas holdups in bubble columns by Hills [11], Ueyama and Miyauchi [12] and Nottenkamper et al. [13]. These studies demonstrate an upward liquid flow up to r/R of about 0.7 and downward flow of liquid in the region from $r/R = 0.7$ to 1. The observations of heat transfer profiles in the present study are generally in agreement with radial profile of liquid velocity in a bubble column. Like the liquid velocities, the heat transfer coefficients are highest at the center and decrease towards the wall. It should be noted, however, that the heat transfer coefficients are also affected by local turbulence created by bubble wake dynamics. For example, the absolute liquid velocity is generally lowest at r/R of about 0.7 (the inversion point) but the heat transfer coefficient is lowest near the wall. This can be attributed to different levels of turbulence at the two locations; higher level of turbulence at r/R of 0.7 results in higher heat transfer coefficients, while dampening effect of the wall would reduce turbulence in the wall region.

3.1. Flow direction

Identification of flow direction and estimation of local liquid or slurry velocities are two important measurements to elucidate flow patterns in a bubble column. The technique used in this study could identify flow direction of liquid from time-averaged local heat transfer coefficients obtained in different probe orientations. The heat transfer coefficients were obtained for three probe orientations: downward (0°), lateral (90°) and upward (180°) orientations. Figs. 7a and b show results obtained in 10 vol.% slurry system at the center and near the wall in bulk region. In the central region, heat transfer coefficients in the downward orientation are higher than those in the upward orientation. Close to the wall, heat transfer coefficients in upward orientation are higher than those in the downward orientation (reverse of the central region). The heat transfer coefficients in the lateral orientation are in between upward and downward orientations (Figs. 7a and b). These observations can be explained based on the formation of boundary layer along the cylindrical probe surface. A boundary layer is formed when a fluid flows over a solid surface since the fluid velocity at the surface is zero. Boundary layer is generally defined as the region of fluid close to the solid surface whose velocity is less than 1% of the free stream velocity [14]. For flow past a cylinder, the development of boundary layer begins with a stagnation point in front of flow and reaches a maximum thickness until a favorable pressure gradient exists in the direction of flow. The boundary layer can separate at the rear end of the probe due to an adverse pressure gradient (i.e. pressure is increasing in the direction of flow). The thickness of thermal boundary layer is smallest in front (near stagnation point) due to the

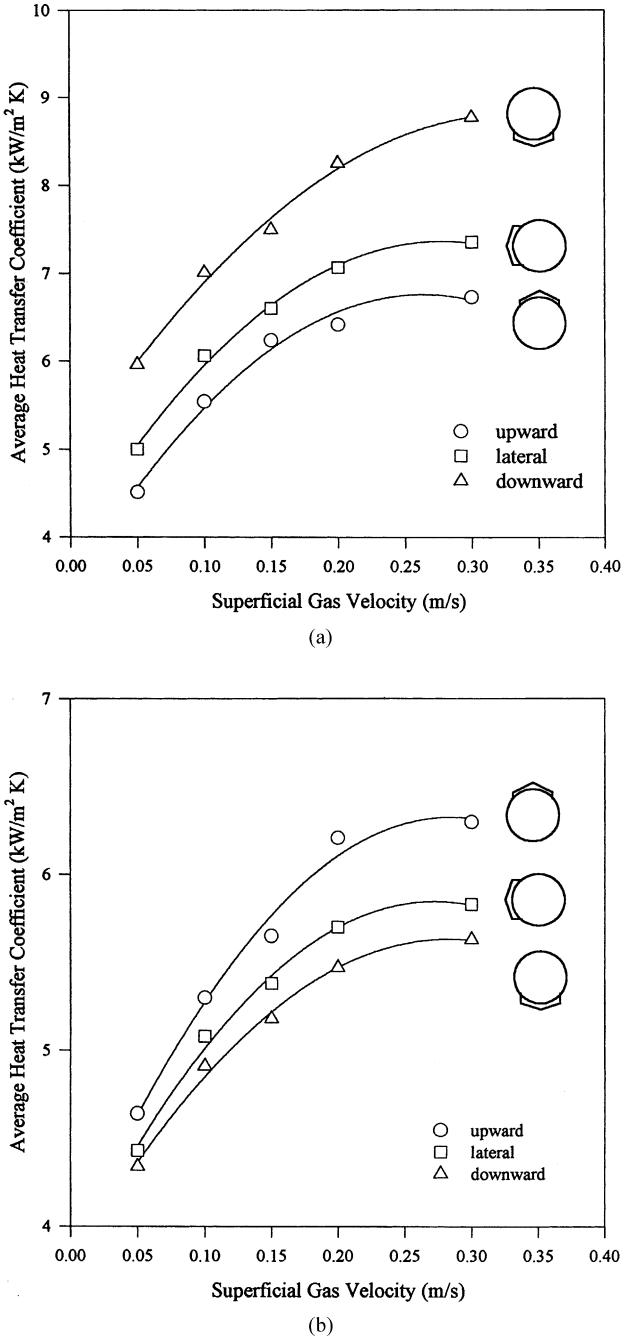

Fig. 7. Local heat transfer coefficients for different probe orientations in: (a) bulk region ($r/R = 0.0$, $z = 1.28$ m, slurry concentration = 10 vol.%); (b) wall region ($r/R = 0.96$, $z = 1.28$ m, slurry concentration = 10 vol.%).

beginning of formation of the thermal layer. The heat transfer coefficients are highest in the downward orientation in the central region (Fig. 7a) indicating an upward fluid flow. The cold water or slurry first arrive at the downside of the heat transfer probe associated with bubble wake. Thus, the bottom of the probe is in front of the incoming flow and it is more frequently renewed by the cold fluid in bubble wake. At the lateral orientation of the probe (90°), a higher boundary layer thickness is formed resulting in a lower heat

transfer coefficient. As shown in Fig. 7a, the heat transfer coefficients at 90° orientation are systematically lower than those in downside orientation at the column center. The heat transfer coefficients in the upward orientation are the lowest where the boundary layer separation effects could influence the heat removal rate. At the wall, the heat transfer coefficients are highest when the probe is facing upwards indicating that flow is downward (Fig. 7b). The downward flow in the wall region of a bubble column has been recorded in the literature [11,12]. These observations show that by measuring heat transfer coefficients at different orientations, the direction of flow of the fluid can be identified in the column thus providing further information about flow patterns.

In the distributor region, there is no significant variation of heat transfer coefficients for different probe orientations in the air–water system (Fig. 8a). This indicates the absence of or low rates of net liquid flow in any one direction in the region. This also indicates low exchange rate of liquid between the distributor and the adjacent region. In 10 vol.% slurry, however, the heat transfer coefficients were higher for probe facing downward at gas velocities higher than 0.15 m/s (Fig. 8b). This behavior could be attributed to a lateral velocity component induced by mixing pattern created by larger bubbles/gas jets formation in the region under these conditions.

3.2. Local liquid/slurry velocity

Significant and systematic differences between local heat transfer coefficient for different probe orientations indicate net liquid flow in one direction. For such conditions, the local heat transfer coefficient at the forward point of stagnation could be used to determine local liquid or slurry velocity. Nusselt number at the forward point of stagnation has been correlated to Reynolds number in single phase flow and empirical equations like the following have been proposed [15]:

$$\frac{h_s d_p}{k} = a_s (Pr)^{0.4} \left(\frac{U_L d_p}{\nu} \right)^{0.5} \quad (3)$$

where a_s is an empirical constant whose value would depend on several factors such as probe design, orientation, etc. Eq. (3) could be used to estimate local free stream velocity provided the value of constant a_s was known. While values of a_s for single phase flow are reported in literature, no such attempts have been made in multiphase systems. In this study, the value of the constant a_s was estimated based on measured local-averaged heat transfer coefficients and available literature data on local liquid velocity in two phase gas–liquid system. Several literature studies have reported local liquid velocities in bubble columns for air–water system [11,13]. The value of the empirical constant was estimated based on local heat transfer coefficient for a commonly used superficial gas velocity of 0.1 m/s and average value of liquid velocity at column center from literature studies. Subsequently, this value of a_s (=0.84) was used

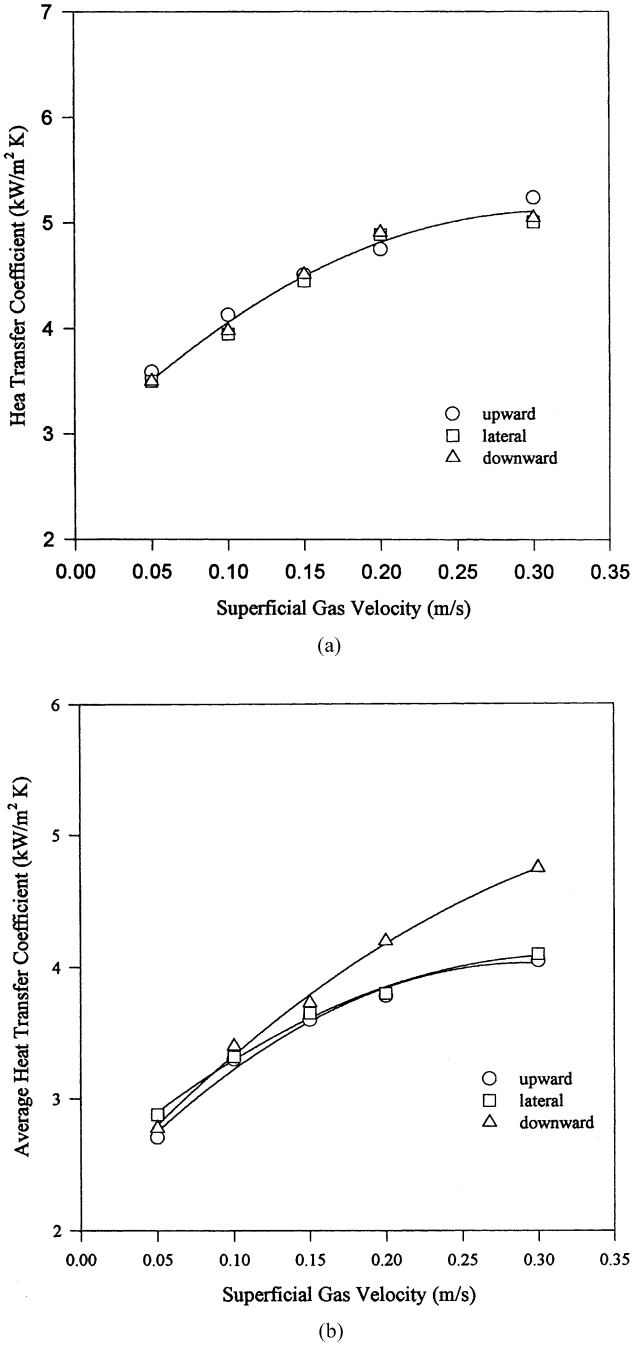

Fig. 8. Variations of heat transfer coefficients in the distributor region for different probe orientations in: (a) air–water system ($z = 0.07$ m, $r/R = 0.5$); (b) 10 vol.% slurry ($z = 0.07$ m, $r/R = 0.96$).

to estimate liquid velocities at the center and near the wall in the bulk region for other superficial gas velocities used in this study. The calculated liquid velocities for these gas velocities were compared with measured values reported in literature studies [11,13]. The predictions were within 10% indicating that the estimate of a_s was reasonable. Literature studies have also proposed equations for estimation of axial liquid velocities in bubble columns. Ueyama and Miyauchi [12] and Wachi et al. [16] developed models for turbulent

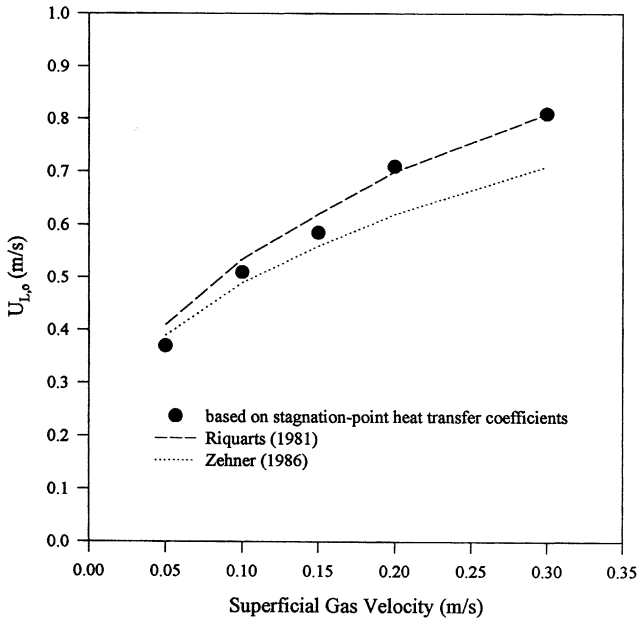

Fig. 9. Comparison of experimental liquid velocities with predictions by literature models (air–water system).

circulation in bubble columns based on momentum balance. Resulting equations, however, require knowledge of local gas holdup, wall shear stress, turbulent viscosity, etc. to calculate local liquid velocity. Riquarts [17] simplified the model of Ueyama and Miyauchi [12] by neglecting the effect of wall friction on the pressure gradient and by introducing a theoretically derived relationship for turbulent viscosity. As a result, the following equation was obtained for the liquid velocity at column axis:

$$U_{\mathrm{L},0} = 0.18\sqrt{gD_{\mathrm{c}}}\left(\frac{V_{\mathrm{G}}^2}{\nu_{\mathrm{L}}g}\right)^{1/8} \tag{4}$$

This simplified model does not require knowledge of the radial profile of gas holdup. The predictions of liquid velocities at the column axis are shown in Fig. 9. A relatively simple model developed by Zehner [18] in the form of multiple circulation cells has also been found to provide reasonable predictions of the liquid velocity at the column center. The calculated values by this model (Eq. (5)) are also compared in Fig. 9.

$$U_{\mathrm{L},0} = \sqrt[3]{\frac{1}{2.5}\frac{\rho_{\mathrm{L}}-\rho_{\mathrm{G}}}{\rho_{\mathrm{L}}}gD_{\mathrm{c}}V_{\mathrm{G}}} \tag{5}$$

It can be seen from Fig. 9 that the predictions obtained upon using the model of Riquarts [17] are within 10% of experimental values obtained in this study. It may be noted that these observations are similar to those recently reported by Krishna et al. [19]. This shows that the approach presented in this study provides reasonable estimates of local liquid velocity in the bubble column. The local circulation velocities in the slurry bubble column were also estimated based on measured stagnation point heat transfer coefficient and Eq. (3). The calculated slurry velocities could not be compared with any measured values due to the absence of such data in literature studies. The slurry velocities were compared with the estimations provided by the energy balance model of Joshi and Sharma [20,21]. Their model assumes existence of multiple cells in the column. The height of each cell was assumed to be equal to column diameter based on minimum continuous phase vorticity in the column. The model was used to develop the following equation for liquid or slurry velocity at column axis in a three-phase sparged column.

$$U_{\mathrm{L},0} = 1.18\left[gD_{\mathrm{c}}\left\{V_{\mathrm{G}} - \varepsilon_{\mathrm{S}}V_{\mathrm{S}} \times \left(\frac{\rho_{\mathrm{S}}}{\rho_{\mathrm{S}}\varepsilon_{\mathrm{S}} + \rho_{\mathrm{L}}\varepsilon_{\mathrm{S}}} - 1\right) - \varepsilon_{\mathrm{G}}U_{\mathrm{b},\infty}\right\}\right] \tag{6}$$

The values of hindered particle settling velocities (V_{S}) and terminal bubble rise velocities ($U_{\mathrm{b},\infty}$) were obtained from Li [9]. The predicted slurry velocities by the above model were generally within 10% of the estimations obtained in this study.

The observations regarding mixing behavior in this study can be compared with literature studies which have investigated flow patterns in bubble columns based on liquid flow profile and mixing measurements [5,6,10,13,22]. These studies demonstrate that at high gas velocities, most of the column is occupied by a large-scale liquid circulation cell with liquid ascending along the core central region and descending along the annular region between the core and the wall. The radioactive particle tracking technique used by Devanathan [23] and Degaleesan et al. [6,7] pointed out different mixing patterns in the distributor and bulk regions of the column. The distributor region was characterized by two- and three-dimensional velocity profiles. Degaleesan et al. [6] proposed a recirculation and cross flow with dispersion (RCFD) model and divided the bubble column axially into three sections. In the middle section, liquid mixing was described by RCFD model and two end zones (i.e. the distributor region and disengagement zone) were assumed to be perfectly mixed. Measurements in this study, however, indicate the presence of a developing region as well, which should be included in the description of a bubble column flow model. The mixing parameters in the developing region can be quite different from the distributor region. Based on the observations in this study, a phenomenological mixing model can be summarized as below:

1. A distributor region which can be assumed to be well mixed (specially at high gas velocities) exists at the column bottom. This region is dominated by the processes of gas bubbles and gas jets formations. It is characterized by low heat transfer rates indicating slow mixing and exchange rates.
2. The developing region above the distributor region has higher mixing rate as demonstrated by higher heat

transfer coefficients in the region. This region is dominated by the process of bubble wake development. The mixing in this region is aided by flow of liquid or slurry from down flowing wall region into the developing wake region. The upward turning flow in this region would reduce possibility of exchange between the distributor and the developing region. For most practical purposes, it may be reasonable to assume this region to be well mixed. More accurate determination of the heights of the distributor and developing regions is possible by additional measurements in this region.

3. The bulk region is characterized by large variation in radial but little variation in axial heat transfer coefficients. This region can be divided into a central core region with an ascending mean liquid or slurry flow and an annular region along the wall with a mean descending flow (like the RCFD model). With increasing gas velocities, the annular flow is extended to lower elevations. It seems that the down flowing liquid is mostly entrained up the column via the developing region. The flow behavior in the core and annular regions could be represented by plug flow with axial dispersion term. The exit region above the bulk region could be assumed to be well mixed.

4. Concluding remarks

Local heat transfer measurements presented in this study can be used to elucidate flow structure in different regions of bubble columns. The technique used in this study can provide local liquid velocity and flow direction. These measurements verify the generally observed flow patterns and mixing behavior discussed in literature in bubble columns. The need to separate the distributor and developing regions for modeling purposes is pointed out. The technique and approach presented in this study can be used to compare the effects of alternative designs on flow patterns and local mixing characteristics in multiphase systems. Moreover, the technique can be combined with tracer studies to develop detailed mathematical description of a phenomenological flow model in multiphase columns.

Acknowledgements

This research project was supported by the Natural Science and Engineering Research Council of Canada (NSERC) through individual research grants awarded to Dr. A. Prakash.

References

[1] L.S. Fan, Gas–Liquid–Solid Fluidization Engineering, Butterworths, Boston, MA, 1989.
[2] R.C. Chen, J. Reese, L.S. Fan, AIChE J. 40 (1994) 1093.
[3] J. Reese, L.S. Fan, Chem. Eng. Sci. 49 (1994) 5623.
[4] R.F. Mudde, J.S. Groen, H.E.A. Van Den Akker, Chem. Eng. Sci. 52 (1997) 4217.
[5] N. Devanathan, D. Moslemian, M.P. Dudukovic, Chem. Eng. Sci. 45 (1990) 2285.
[6] S. Degaleesan, S. Roy, S.B. Kumar, M.P. Dudukovic, Chem. Eng. Sci. 51 (1996) 1967.
[7] S. Degaleesan, M.P. Dudukovic, B.A. Toseland, B.L. Bhatt, Ind. Eng. Chem. Res. 36 (1997) 4570.
[8] H. Li, A. Prakash, Ind. Eng. Chem. Res. 36 (1997) 4688.
[9] H. Li, Ph.D. Thesis, The University of Western Ontario, London, Ont., 1998.
[10] R. Krishna, J.W.R. deSwart, J. Ellenberger, G.B. Martina, C. Maretta, AIChE J. 43 (1977) 311.
[11] J.H. Hills, Trans. Instn. Chem. Eng. 52 (1974) 1.
[12] K. Ueyama, T. Miyauchi, AIChE J. 25 (1979) 258.
[13] R. Nottenkamper, A. Steiff, P.M. Weinpach, Ger. Chem. Eng. 6 (1983) 143.
[14] R.S. Brodkey, H.C. Hershey, Transport Phenomena—A Unified Approach, McGraw-Hill, New York, 1988.
[15] E.W. Comings, J.T. Clapp, J.F. Taylor, Ind. Eng. Chem. 40 (1948) 1076.
[16] S. Wachi, H. Morikawa, K. Ueyama, J. Chem. Eng. Jpn. 20 (1987) 309.
[17] H.P. Riquarts, Ger. Chem. Eng. 4 (1981) 18.
[18] P. Zehner, Int. Chem. Eng. 26 (1986) 22.
[19] R. Krishna, M.I. Urseanu, J.M. van Baten, J. Ellenberger, Chem. Eng. Sci. 54 (1999) 4903.
[20] J.B. Joshi, M.M. Sharma, Trans. Instn. Chem. Eng. 57 (1979) 244.
[21] J.B. Joshi, M.M. Sharma, Trans. Instn. Chem. Eng. 60 (1982) 255.
[22] Z. Yang, U. Rustemeyer, R. Buchholz, U. Onken, Chem. Eng. Commun. 49 (1986) 51.
[23] N. Devanathan, D.Sc. Dissertation, Washington University, Saint Louis, MO, 1991.